Journal of Materials Processing Technology 210 (2010) 2215–2222

Contents lists available at ScienceDirect

Journal of Materials Processing Technology

journal homepage: www.elsevier.com/locate/jmatprotec

Experimental investigation and 3D finite element prediction of the heat affected zone during laser assisted machining of Ti6Al4V alloy

Jihong Yang[a,*], Shoujin Sun[a], Milan Brandt[b], Wenyi Yan[c]

[a] CAST Cooperative Research Centre, Faculty of Engineering and Industrial Sciences, Swinburne University of Technology, PO Box 218 (H66), Hawthorn, VIC 3122, Australia
[b] School of Aerospace, Mechanical and Manufacturing Engineering, RMIT University, Bundoora, VIC 3083, Australia
[c] Department of Mechanical and Aerospace Engineering, Monash University, Clayton, VIC 3800, Australia

ARTICLE INFO

Article history:
Received 18 April 2010
Received in revised form 10 August 2010
Accepted 12 August 2010

Keywords:
Finite element method
Titanium alloy
Thermomechanical processing
Laser heating
Heat affected zone

ABSTRACT

An experimental study was conducted to characterize the heat affected zone produced when laser heating a Ti6Al4V alloy plate workpiece. The emissivity and absorptivity of the Ti6Al4V alloy were determined experimentally. A 3D transient finite element method for a moving Gaussian laser heat source was developed to predict the depth and width of the heat affected zone on the Ti6Al4V alloy workpiece. There was a close correlation between the experimental data and the simulation results. It was found that the depth and width of the heat affected zone were strongly dependent on the laser parameters (laser power, laser scan speed, the angle of incidence and the diameter of the laser spot) and material properties (thermal conductivity, specific heat and density). Parametric studies showed that the depth and width of the heat affected zone increased with an increase in the laser power and decreased with an increase of the laser spot size and the laser scan speed. The thermal model can be used to determine the laser parameters for a given cut geometry that will yield no residual heat affected zone in the material after cutting. This provides the basis to optimize and improve laser assisted machining technique.

1. Introduction

Titanium alloys have been widely used in aerospace, biomedical and automotive industries because of their high strength-to-weight ratio and superior corrosion resistance at room and elevated temperatures. Ti6Al4V is the most popular titanium α–β alloy – its total production is about half of all titanium alloys. Aluminum (Al) is added to the alloy as the α-phase stabilizer and hardener due to its solution strengthening effect. Vanadium (V) stabilizes the ductile β-phase, providing hot workability of the alloy. However, titanium alloys are difficult to machine due to their high strength, low thermal conductivity and high chemical reactivity. Rahman et al. (2006) concluded that conventional machining of titanium alloys is a low productivity process with high materials running costs, such as the costs of tool and coolant.

Laser assisted machining (LAM) of aerospace alloys was initially suggested by Rajagopal et al. (1982). Laser assisted hot machining of ceramics was developed by Konig and Zaboklicki (1993). Chryssolouris et al. (1997) reported that LAM had been considered as an alternative to conventional machining of hard and/or difficult-to-process materials. Since 1982 the LAM technique have been used to machine such as stainless steel (Anderson and Shin, 2006), Inconel 718 (Anderson et al., 2006), titanium alloys (Sun et al., 2008) metallic alloys and silicon nitride ceramics (see, e.g., Lei et al., 1999; Rozzi et al., 2000). During the LAM process a laser beam heats the workpiece material directly ahead of a conventional cutting tool. The heat from the laser beam reduces the strength of the workpiece material along the machine tool path. Therefore, the material can be cut more easily with a lower cutting force. As a result, LAM leads to a higher material removal rate, an increased productivity, and a longer tool life when compared with conventional machining.

A major feature of the LAM process is the number of parameters, which must be controlled during cutting. In addition to the conventional cutting parameters (cutting speed, feed rate, depth of cut, type of tool), there are laser parameters and also the interaction parameters between the relative position of the laser beam and cutting tool. Modeling of LAM is of great importance, since a better process understanding will allow process optimization and control. An accurate model of an underlying experimental system is necessary to conduct parametric studies to characterize the temperature distribution during thermally assisted machining. Furthermore, this heat-assisted process induces a detrimental heat affected zone (HAZ) in the part. The HAZ can be determined from the investigation of the laser heating, which can assist the design of the following machining so that the entire HAZ can be removed by machining.

* Corresponding author. Tel.: +61 3 92144342; fax: +61 3 92145050.
E-mail address: jyang@swin.edu.au (J. Yang).

0924-0136/$ – see front matter © 2010 Elsevier B.V. All rights reserved.
doi:10.1016/j.jmatprotec.2010.08.007

Table 1
Chemical composition of Ti6Al4V (Grade 5) as mass percentage.

N	C	H	Fe	O	Al	V	Ti
0.05	0.08	0.015	0.40	0.20	5.5–6.75	3.5–4.5	Bal.

To date, Kou et al. (1983) used the Fourier differential equation to predict the depth of the HAZ during laser heating which were used in most of the models. Bokota and Iskierka (1996) found that this method was quite difficult to solve analytically for given boundary and initial conditions. Ashby and Easterling (1984) carried the analytical analysis further, developing an approximate solution for the entire temperature field. Pantelis and Vonatsos (1998) have developed a new analytical thermal model that uses a Taylor series approximation to estimate the HAZ in the case where no melting occurs. Also, they developed a new analytical thermal model for the case where melting occurs, by using a moving-front approach. The major disadvantage of the above methodology was the complexity of the solutions. The FEM for numerical evaluation is another approach for heat flow modeling applied to a moving heat source, which has been developed by Rosenthal (1946). The FEM analysis allows us to easily vary thermal properties, obtain the results thoroughly and consider any heat flux. Germain et al. (2007) have used the FEM thermal numerical simulation to predict the size and shape of the HAZ in two metals (100Cr6/AISI 52100 and Ti6Al4V) during moving laser irradiation by using a commercial finite element package Abaqus/Standard®. Also a FEM model was developed to predict the HAZ caused by laser heating of H-13 model/die steel (42 HRC) in the laser assisted micromachining by Singh et al. (2008). Yang et al. (2009) have developed a 3D FEM model to predict the HAZ in the Ti6Al4V plate workpiece by a moving Gaussian laser beam.

This study focuses on the characterization and prediction of the HAZ caused by laser heating of Ti6Al4V alloy process. The HAZ produced by laser heating at different laser parameters was observed and analyzed experimentally by using metallographic methods. The emissivity and absorptivity of the Ti6Al4V alloy plate workpiece were investigated from the experimental work. A 3D transient finite element thermal model for a moving Gaussian laser beam was developed to predict the temperatures generated in the workpiece and validated by comparing with experimentally measured temperature data. A spatial temperature range corresponding to the formation of the HAZ and the depth of HAZ was then identified and validated by experimental observations.

This model not only can be used to predict the HAZ parameters for the Gaussian laser beam profile, but also for other intensity laser profiles such as flattop or inverse Gaussian beam in real industrial applications. In the future work we will consider using beam shaping technique reported by Alexander (2006) to convert the Gaussian beam into flattop profile to reduce the HAZ in laser assisted material cutting processing.

2. Experimental procedure and results

2.1. Experimental procedure

Experiments were conducted to characterize the HAZ produced in laser heating without mechanical cutting. The workpiece is a Ti6Al4V alloy plate with a width of 170 mm, a length of 227 mm and a thickness of 6.5 mm. The chemical composition of Ti6Al4V alloy is given in Table 1. A Rofin-Sinar 2.5 kW Nd:YAG laser system was utilized to generate a laser beam. The laser beam was transmitted along a 10 m long step-index optical glass fibre of 0.6 mm diameter terminated with a collimating optic. The beam was reflected to the workpiece by a mirror inclined at 45° in the bending cube. The laser beam was focused on the surface of the plate with a focussing lens of 200 mm focal length. The lens position was chosen to produce spot diameters from 2.0 to 4.4 mm on the surface of the plate.

Fig. 1 shows a schematic illustration of the laser heating experiment. The spot temperature was measured by a Maurer KTR 1075, two-colour pyrometer with a response time of 20 μs and temperature range of 800–2500 °C. An infra-red thermal camera was also used to monitor the surface temperature distribution produced by the moving laser beam and had a temperature range of 300–2200 °C. The plate temperature was measured using CO1 and CO2 K-type thermocouples with response times of 10–20 and 2–5 ms respectively. These thermocouples were cemented onto the top and bottom faces of the plate at different points adjacent to the beam path. The plate was sectioned after laser heating, ground and polished. Microhardness testing was performed across the treated path to examine the variation of hardness due to the change in the microstructure. The hardness was carried out with a load of 50 g with a loading time of 15 s. The polished sample was etched with the Kroll's reagent and the microstructure in the heated track was examined using optical microscopy.

2.2. Experimental results of emissivity and absorptivity measurements

Emissivity (ε) is a term representing a material's ability to emit thermal radiation. Each material has a different emissivity and it can be quite a task to determine the appropriate emissivity for

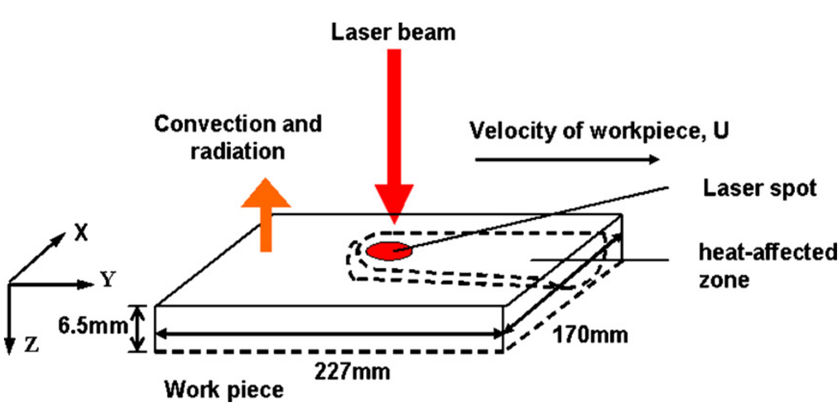

Fig. 1. A schematic illustration of the laser heating experiment.

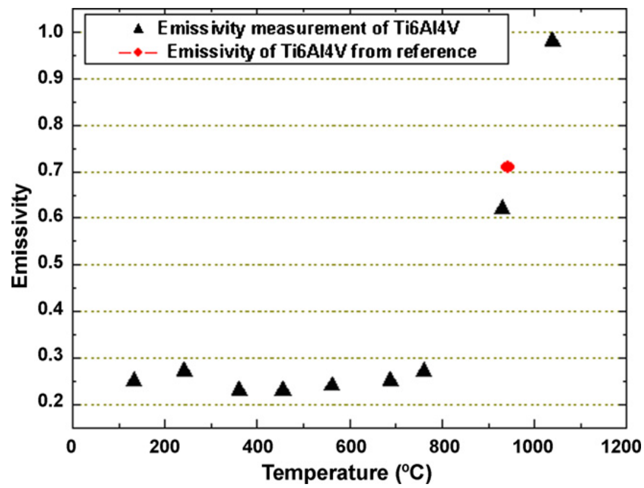

Fig. 2. Measured emissivity values at different temperatures on the Ti6Al4V plate sample, compared with a reference value from Coppa and Consorti (2005).

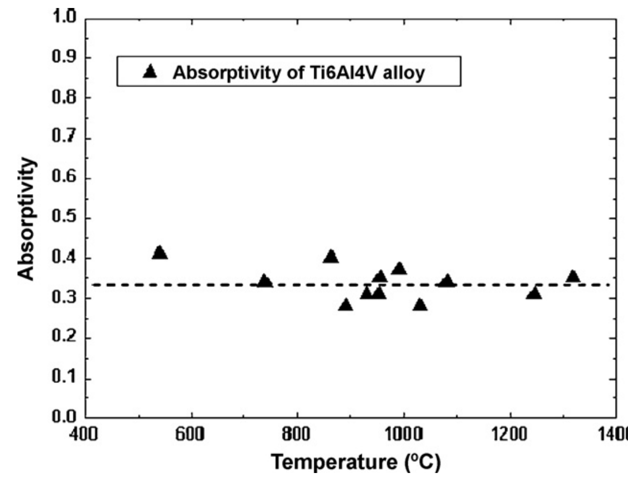

Fig. 3. The results of absorptivity versus temperature behavior of the Ti6Al4V plate sample.

a subject. The value of ε is generally obtained from measuring the sample (T_s) and its radiance temperature (T_r) via (Coppa and Consorti, 2005),

$$\varepsilon = \left(\frac{T_r}{T_s}\right)^4 \quad (1)$$

In our experiment, T_s was measured using a K-type thermocouple which was cemented on the back face of the plate at a point 3 mm from the laser beam centre. T_r was measured using a FLIR infra-red thermal camera, looking at the back face of the plate. The ε was obtained from T_s and T_r by the infra-red thermal camera calculation.

Fig. 2 shows measured emissivity values which vary from 0.25 to 0.98 over the temperature range of 132–1029 °C on the Ti6Al4V plate sample. It is evident that in the low temperature range, below 760 °C, the emissivity is almost independent of temperature. At the temperature above 760 °C, Ti6Al4V alloy starts to oxidize and its emissivity increases rapidly. Coppa and Consorti (2005) have found the emissivity value of 0.708 ± 0.012 which was measured at 943 °C during the cooling (red dot in Fig. 2). As we can see, the reference value is within the range of our measured data.

Absorption is an important phenomenon during laser heating, affecting the process efficiency and reliability, but it has been studied little due to its complex nature. Recently, we have developed an indirect method for calculating absorptivity (A) by using analytical method with experimental measured maximum temperature on the top surface of the workpiece material. The temperature at top surface during heating has been described by Dahotre and Harimkar (2007) given by Eq. (2):

$$\Delta T(0,t) = \frac{q}{k}\sqrt{\frac{4\alpha t_p}{\pi}} \quad (2)$$

where k and α are the thermal conductivity and thermal diffusivity respectively. q is the absorbed laser intensity. It can be given by the product of absorptivity A and incident laser intensity $P/\pi b^2$ (i.e., $q = A(P/\pi b^2)$), P the incident laser power, b the value of laser spot radius, t_p the laser pulse time ($t_p = 2b/U$).

Therefore the absorptivity A can be obtained as follows:

$$A = \frac{k\Delta T}{2P}\sqrt{\frac{\pi^3 b^3 U}{2a}} \quad (3)$$

The Ti6Al4V plate sample tests were carried out at five laser scanning speed (33.33, 66.66, 100, 133.3 and 166.6 mm/s) and eight laser power levels (500, 750, 1000, 1250, 1500, 1750, 2000 and 2380 W). In this case the beam radius b is 3.1 mm, the thermal conductivity k is 7 W/mK and thermal diffusivity a is $2.9 \times 10^6\ \mathrm{m^2/s}$. Absorptivity obtained by this method was between 0.28 and 0.41 over the temperature range 500–1400 °C, below the melting point (1650 °C) of the Ti6Al4V plate sample (see Fig. 3). Therefore, the average absorptivity $A = 0.34$, of the Ti6Al4V plate workpiece was used in the following FEM simulation.

2.3. Experimental results of characterization of HAZ

In this work, laser heating was studied without machining. The titanium alloy (Ti6Al4V) was tested at five laser scanning speeds and six laser power levels (see Table 2).

Five different microstructure zones were investigated (see Fig. 4): a melted zone with dendritic microstructure (layer A), a needle-shaped zone (layer B, single martensite phase, α'), a fine needles-shaped zone (layer C, single martensite phase, α'), a lamellar zone (layer D, $\alpha + \alpha'$) and an equiaxed zone (layer E, $\alpha + \beta$). Both layers B and C are formed by rapid cooling from the temperature where only the single beta phase exists, i.e. above the beta transit temperature, which is about 980 °C. The first three zones are collectively called the heat affected zone (HAZ) as shown in Fig. 4. The phase composition changes from layer A to layer D along the depth of track due to the temperature gradient. The measured maximum temperature (T_{Max}) on top of the workpiece surface, maximum width (Wc) of HAZ and depth of HAZ (Lc) was given in Table 2.

Indentation hardness was carried out after the specimen cooled down to room temperature. The variation in hardness across the track is shown in Fig. 5 with the corresponding microstructure. Hardness drops rapidly from 606 Hv in melt layer A to 420 Hv in layers B, C and D and keeps decreasing to 360 Hv below layer D.

In the Ti6Al4V alloy, it was found that the depth of HAZ increases with increasing laser power and decreases with increasing laser spot size and laser scan rate. Germain et al. (2007) was also conducted the experiments at two speed 26 and 53 mm min^{-1} and four laser power levels 0.5, 1, 1.5, 2 kW in Ti6Al4V alloy. Four different micro-structural were found, a melted zone, a zone characterized by needle-shaped structure, a lamellar zone and an equiaxed zone (annealed state). The first three zones correspond to the heat affected zone. Germain et al. (2007) also carried out the microhardness tests and reported on the various microstructures. Dendritic and fine needle-shaped microstructures have hardness values higher than that of the initial equiaxed microstructure.

Table 2
Laser heating test parameters and measured maximum width, and depth of HAZ.

Case	P (W)	U (mm/s)	b (mm)	Max width of HAZ (mm)	Max depth of HAZ Lc (mm)
1	893	39.06	2.2	2.23	0.38
2	1381	39.06	2.2	3.45	0.75
11	2042	83.58	2.2	2.82	0.43
12	1381	83.58	2.2	2.09	0.31
21	893	50.28	2.2	2.07	0.34
22	1381	50.28	2.2	3.29	0.63
23	678	17.35	2.2	3.26	0.83
24	447	12.75	2.2	2.98	0.70
25	1778	83.58	2.2	2.72	0.44
26	1778	116.67	2.2	2.18	0.30
28	1381	116.67	1.0	1.79	0.35
32	1621	116.67	2.2	1.90	0.27
34	1778	166.25	2.2	1.43	0.17

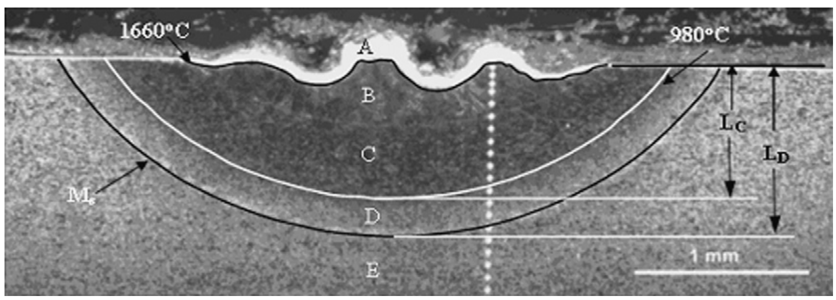

Fig. 4. Microstructure transition in the heat affected zone for Ti6Al4V alloy and constructed temperature contours for the case 23.

3. Thermal modeling

3.1. Physical description of the model

A schematic illustration of laser heating trial is showing in Fig. 1. The laser beam and the coordinate system are fixed and the workpiece moves at velocity U. The origin of an x–y–z coordinate system was chosen at the centre of the laser beam on the work piece surface. The depth of the work piece was aligned in z direction and increases with increasing z.

In this work, the estimation of heat treatment is based on the following assumptions:

(1) The laser beam is regarded as a base mode Gaussian beam perpendicularly directed at the top surface of the workpiece.
(2) The Gaussian distribution of absorbed laser heat flux $q(x, y)$ is given by Dahotre and Harimkar (2007):

$$q(x,y) = \frac{2P}{\pi b^2}\exp\left(-\frac{2(x^2+y^2)}{b^2}\right) \quad (4)$$

(3) The average absorptivity of the Ti6Al4V plate workpiece is 0.34.
(4) The thermo-physical properties of the workpiece material are shown in Table 3 (Mills, 2002).
(5) The treated workpiece material is homogeneous.
(6) The ambient temperature is 22 °C.
(7) Air convection coefficient is 50 [W/m^2 K].
(8) In the centre of the laser beam, when the temperature exceeds the melting point (1660 °C) the node remains in the mesh, and the latent heat of the fusion is simulated by artificially increasing the liquid specific heat.

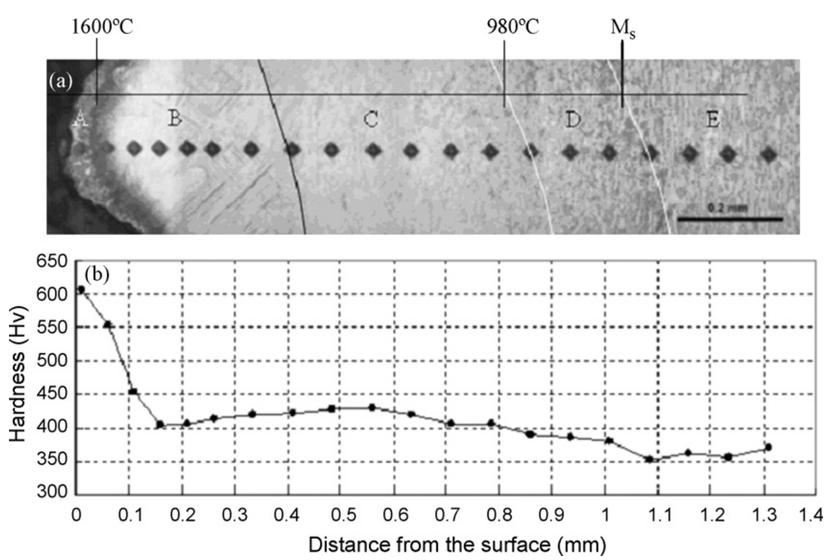

Fig. 5. (a) The indentation on microstructure and (b) hardness across the pre-heated track for the case 23.

Table 3
Thermo-physical properties of Ti6Al4V alloy (Mills, 2002).

Temperature (°C)	Thermal conductivity (W/mK)	Specific heat (J/K kg)	Density (kg/m³)
25	7.0	546	4420
100	7.45	562	4406
200	8.75	584	4395
300	10.15	606	4381
400	11.35	629	4366
500	12.6	651	4350
600	14.2	673	4336
700	15.5	694	4324
800	17.8	714	4309
900	20.2	734	4294
995	19.3	641	4282
1100	21	660	4267
1200	22.9	678	4252
1300	23.7	696	4240
1400	24.6	714	4225
1500	25.8	732	4205
1600	27	750	4198
1650	28.4	759	4189
Uncertainty	±10%	±3%	±3%

3.2. Mathematical description of the model

The 3D transient time-dependent heat conduction in the space underneath the irradiated surface is described by Eq. (5) (Incropera et al., 2006):

$$\rho c_p\left(\frac{\partial T}{\partial t}+U\frac{\partial T}{\partial y}\right)=\frac{\partial}{\partial x}\left(k\frac{\partial T}{\partial x}\right)+\frac{\partial}{\partial y}\left[k\frac{\partial T}{\partial y}\right]+\frac{\partial}{\partial z}\left[k\frac{\partial T}{\partial z}\right]+\dot{Q} \quad (5)$$

where ρ, c_p, k, $\dot{Q}$, U are the density, specific heat, thermal conductivity, power generation per unit volume and the velocity of the work piece, respectively.

The initial condition at time $t = 0$ is given by

$$T(x, y, z, 0) = T_0 \quad (6)$$

The natural boundary condition takes into account the imposed heat flux, radiation and convection at the laser irradiated surface and can be defined by

$$-k\frac{\partial T}{\partial z}=q(x, y)-h(T-T_0)-\sigma\varepsilon(T^4-T_0^4) \quad (7)$$

where heat flux q is normal to the laser irradiated surface, T_0 is ambient temperature; h is heat transfer coefficient for convection, σ is Stefan–Boltzmann constant for radiation (5.67×10^{-8} W/m² K⁴) and ε is emissivity. The temperature-dependent emissivity values for Ti6Al4V alloy (Grade 5) plate workpiece have been determined by selecting a reference point and measuring its temperature using an infra-red thermal camera and a K-type thermocouple (see Fig. 2).

3.3. Finite element model

A thermal numerical simulation was performed to predict the temperature, size and shape of the HAZ. The finite element model was created in ANSYS (version 11.0 SP1). A finer mapped mesh was used in the higher temperature area directly below the incident Gaussian laser heat flux. This fine mesh method enables the calculation of the steep temperature gradients with precision. The mesh consisted of 8-node 3D thermal element. The model contains 184,789 nodes and 124,794 elements. The moving laser beam is symmetric so that the semi-circular Gaussian distribution of heat flux was defined. A plane of symmetry was used therefore only half of the workpiece was modelled. The dimension of the modelled workpiece was of width 10 mm, length 20 mm and thickness 6.5 mm. The initial temperature was 22 °C. The bottom face was maintained at same initial room temperature 22 °C.

4. Results and discussions

4.1. Three dimensional model results

The results of the ANSYS program can be displayed in many ways. The 3D temperature distribution is shown for the case 23 of 678 W laser power, 17.35 mm/s laser scan speed and 4.4 mm spot diameter for the different times in Fig. 6.

These results indicate that the temperature distribution decreases very rapidly in the z direction. It can be seen the maximum temperature on the top layer of the workpiece is almost 2269 °C at 0.25 s, which is higher than the melting point temperature (1650 °C) of Ti6Al4V alloy. Therefore, some of the alloy has melted on the top surface of workpiece material. As a result, the top surface of the workpiece does not remain flat practically and shows ripples (refer to Fig. 4).

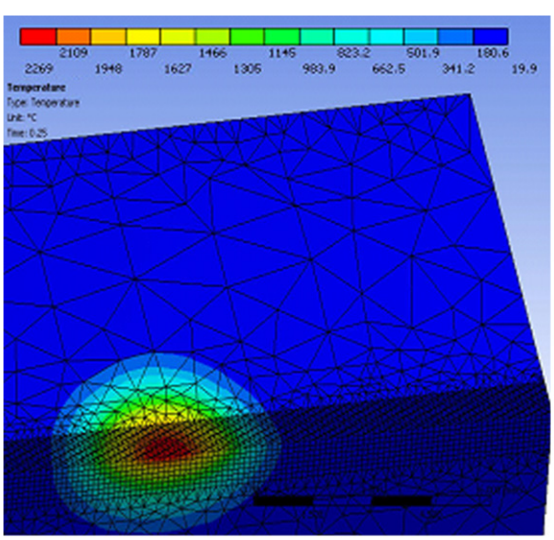

(a) at 0.25s

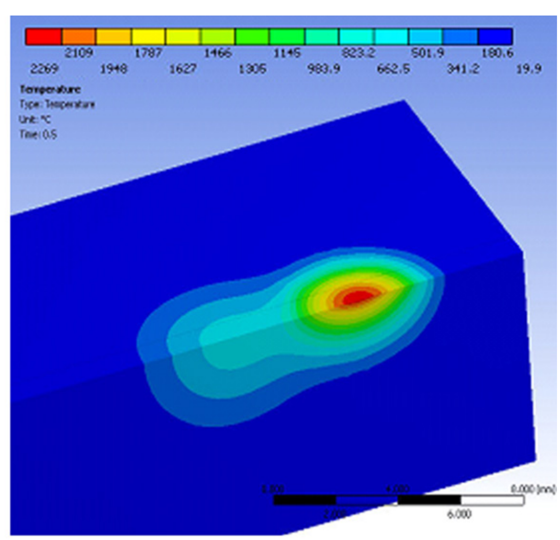

(b) at 0.5s

Fig. 6. The 3D temperature distribution of Ti6Al4V alloy for the case of 678 W laser power and 17.35 mm/s laser scan speed and 4.4 mm laser spot diameters, (a) at 0.25 s, (b) at 0.5 s.

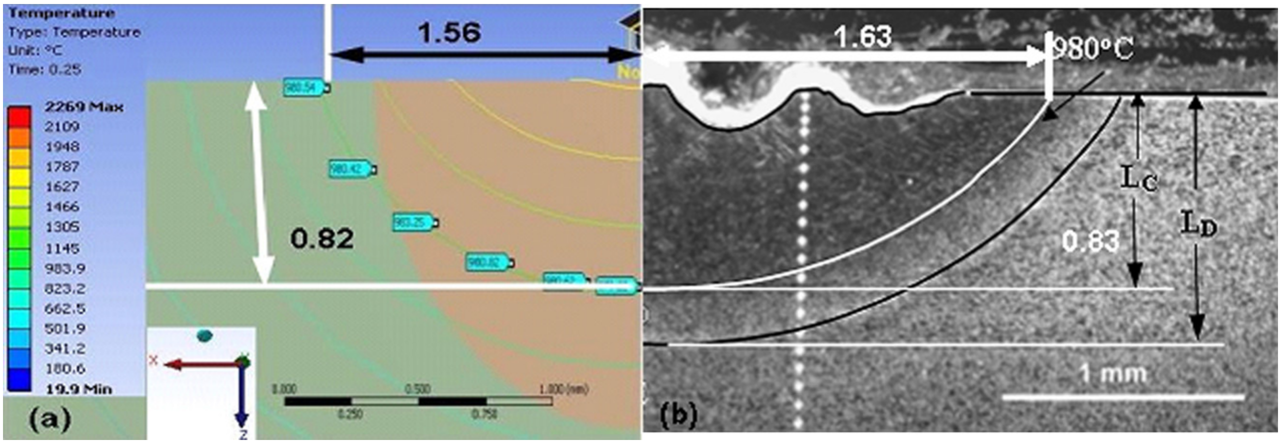

Fig. 7. Comparison of the temperature fields of the simulation and experiment for a 678 W laser power, 17.35 mm/s scan speed, 4.4 mm spot size, (a) FE results, (b) experimental results.

4.2. Comparison with experimental data

The FEM model enables us to define the volume of Ti6Al4V plate workpiece with a 3D temperature contour higher than 980 °C, which corresponds to the HAZ zone where only the single beta phase exists, i.e. above the beta transit temperature. Fig. 7 shows a close correlation between the simulation (Fig. 7(a)) and experimental results (Fig. 7(b)) concerning the prediction of the HAZ. Some slight differences can be seen. The simulation predicts a slightly shallower depth (0.82 mm for simulation, 0.83 mm for experimental) and smaller width (3.12 mm for the simulation, 3.26 mm for the experimental). Therefore, for a given HAZ volume, the shape of the predicted HAZ has less area and volume than the experimentally determined geometry.

Comparison of the simulated and measured maximum depth and width of HAZ for various laser powers (447–2042 W) and laser scan rates (12.75–166.25 mm/s) is given as Fig. 8(a) and (b) respectively. We can see there is good correlation between the simulated and measured results.

4.3. Laser parametric study

To understand the contribution of the laser parameters (laser power, laser scan speed and laser spot radius) on the maximum depth and width of HAZ, a parametrical study was performed for

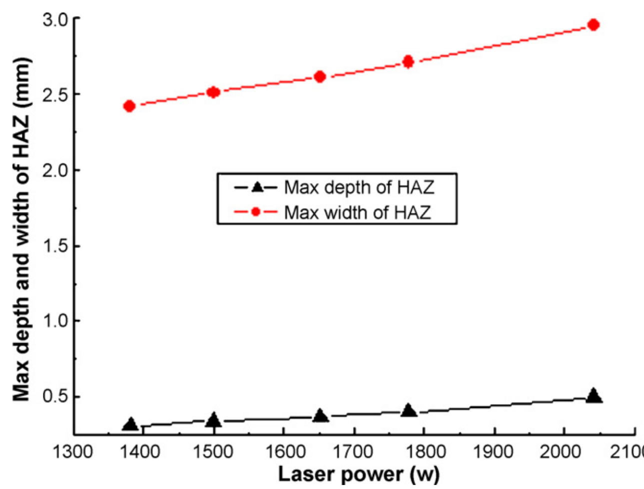

Fig. 9. Maximum depth and width of HAZ versus laser power (operating condition U = 83.58 mm/s; b = 2.2 mm).

different laser parameters. Fig. 9 shows the influence of the laser power parameter, P, on the maximum depth and width of HAZ during laser heating trial. In all the five cases for laser power from 1381, 1500, 1652, 1778–2042 W, the other laser parameters are fixed at

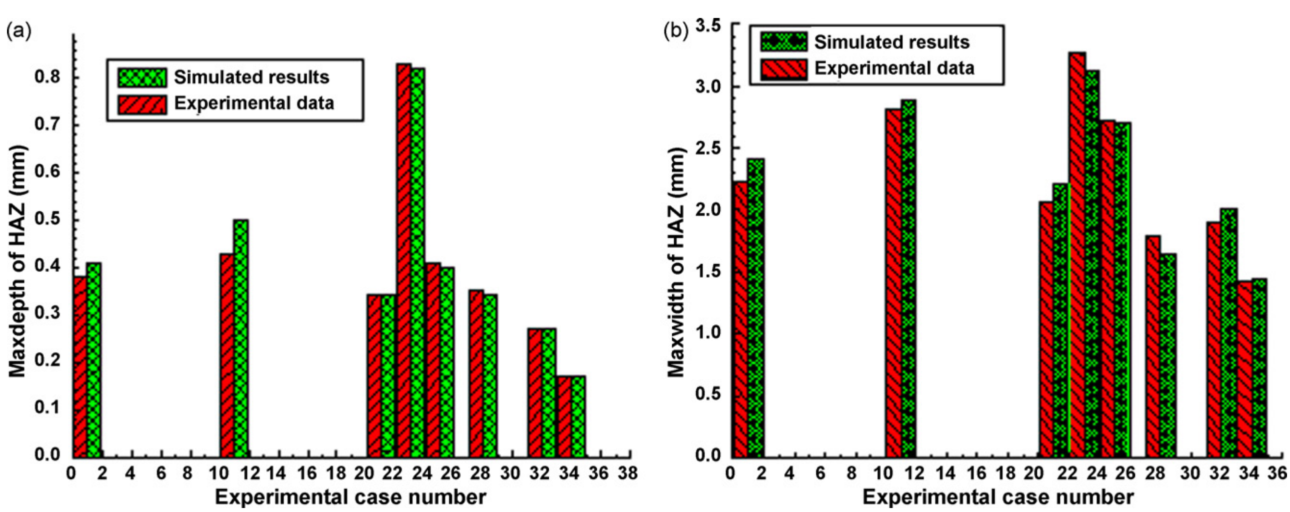

Fig. 8. Comparison of model results to experimental measurements for different cases, (a) maximum depth of HAZ, (b) maximum width of HAZ.

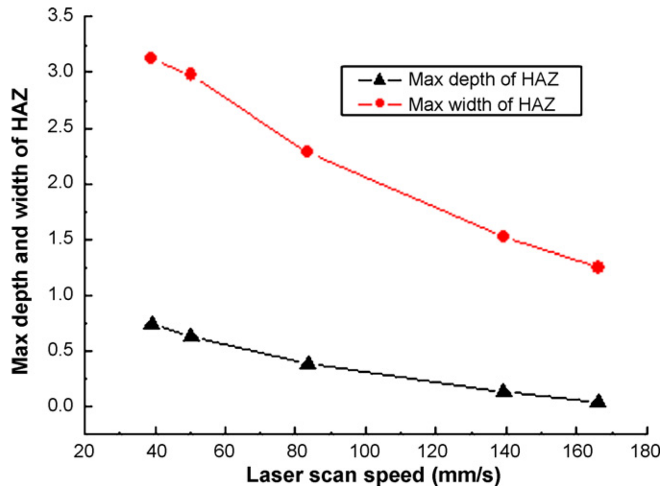

Fig. 10. Maximum depth and width of HAZ versus laser scan speed (operating condition P = 1381 W; b = 2.2 mm).

U = 83.58 mm/s; b = 2.2 mm. As we can see the maximum depth and width of HAZ increase almost linearly with the laser power.

The effect of the laser scans speed, U, on the maximum depth and width of HAZ is given in Fig. 10. It can be seen that for the five laser scan speeds, 39.06, 50.28, 83.58, 139.18 and 166.25 mm/s with fixed laser power, P = 1778 W, and laser spot radius, b = 2.2 mm, the maximum depth and width of HAZ decrease with the increasing laser scan speed.

The influence of the laser spot size, b, on the maximum depth and width of HAZ is shown in Fig. 11 by keeping the same laser power, P = 1381 W, and laser scan speed, U = 116.67 mm/s, for the five different laser spot radii, 1.0, 1.50, 2.20, 2.75 and 3.1 mm. We can see the maximum depth and width of HAZ decrease with the increasing laser spot radius.

The results of the parametric study indicate that the maximum depth and width of HAZ increases almost linearly with the laser power and decreases with the increase of the laser scan speed and laser spot radius. This prediction is consistent with experimental results by Sun et al. (2007). They found that the depth of HAZ increases with the laser power and decreases with the increase of the laser spot size and laser scan speed.

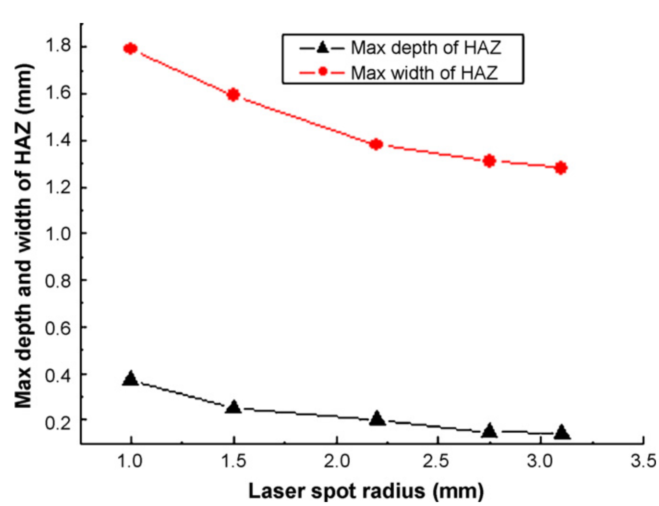

Fig. 11. Maximum depth and width of HAZ versus laser spot radius (operating condition P = 1381 W; U = 116.67 mm/s).

5. Conclusions

The experimental investigation and the finite element analysis were performed to study and predict the volume of HAZ during a moving laser source on a Ti6Al4V alloy plate workpiece. The experimental and FEM simulation results both reveal important relationships between the size of HAZ and laser parameters and material properties. The major conclusions of this study are as follows:

- Two important thermal factors of the Ti6Al4V alloy plate workpiece, namely emissivity and absorptivity were determined by using this experimental and analytical approach.
- Five different microstructures were investigated by laser heating of the Ti6Al4V plate workpiece. They are a melted zone dendritic microstructure, needle-shaped zone, a fine needle-shaped zone, a lamellar zone and an equiaxed zone.
- A transient three-dimensional finite element model (FEM) has been developed to analyze the temperature distribution in the Ti6Al4V alloy workpiece and geometry of the HAZ.
- There is a close correlation between FEM and experiment results. The thermal model accurately predicts the volume of material with temperatures higher than 980 °C, which corresponds to the HAZ.
- Parametric studies show that the depth and width of HAZ increases with the laser power and decreases with the increase of the laser spot size and laser scan speed.
- The thermal model can be used to determine the laser parameters for a given cut geometry that will yield no residual HAZ in the material after cutting.

Acknowledgements

The authors would like to acknowledge the financial support from the CAST Cooperative Research Centre (project no. 5-01-323) and its permission to publish this work. The CAST Cooperative Research Centre was established and is supported under the Australia Government's Cooperative Research Centres Programme.

References

Alexander, L., 2006. Beam shaping? Easy Ind. Laser Sol., July 19.
Anderson, M.C., Shin, Y.C., 2006. Laser-assisted machining of an austenitic stainless steel: P550. Proc. Inst. Mech. Eng. B: J. Eng. Manuf. 220 (12), 2055–2067.
Anderson, M., Patwa, R., Shin, Y.C., 2006. Laser-assisted machining of Inconel 718 with an economic analysis. Int. J. Mach. Tools Manuf. 46, 1879–1891.
Ashby, M.F., Easterling, K.E., 1984. Transformation hardening of steel surface by laser beam. Acta Metall. 32 (11), 1935–1948.
Bokota, A., Iskierka, S., 1996. Numerical prediction of the hardened zone in laser treatment of carbon steel. Acta Mater. 44 (2), 445–450.
Chryssolouris, G., Anifantis, N., Karagiannis, S., 1997. Laser assisted machining: an overview. ASME, J. Manuf. Sci. Eng. 119, 766–769.
Coppa, P., Consorti, A., 2005. Normal emissivity of sample surrounded by surfaces at diverse temperatures. Measurement 38, 124–131.
Dahotre, N.B., Harimkar, S.P., 2007. Laser Fabrication and Machining of Materials. Spring Science+ Business Media, New York, USA, pp. 42–43.
Germain, G., Morel, F., Lebrun, J.L., Morel, A., 2007. Machinability and surface integrity for a bearing steel and a titanium alloy in laser assisted machining. Laser Eng. 17, 329–344.
Incropera, F.P., Dewitt, D.P., Bergman, T.L., Lavine, A.S., 2006. Fundamentals of Heat and Mass Transfer, 6th ed. John Wiley & Sons, New York, pp. 72–73.
Konig, W., Zaboklicki, A.K., 1993. Laser-assisted hot machining of ceramics and composite materials. Proceedings of the International Conference on Machining of Advanced Materials, NIST Special Publication 847, pp. 455–463.
Kou, S., Sun, D.K., Lee, Y.P., 1983. Fundamental study of laser transformation hardening. Metall. Trans. A 14 (4), 643–653.
Lei, S., Shin, Y.C., Incropera, F.P., 1999. Experimental investigation on thermomechanical characteristics in laser-assisted machining of silicon nitride ceramics. Proc. ASME, Manuf. Sci. Eng. Med. 10, 781–788.
Mills, K.C., 2002. Recommended Values of Thermophysical Properties for Selected Commercial Alloys, 1st ed. Antony Rowe Ltd, Wiltshire, England, p. 217.
Rajagopal, S., Plankenhorn, D.J., Hill, V.L., 1982. Machining aerospace alloys with the aid of a 15 kW laser. J. Appl. Metalworking 2 (3), 170–184.

Pantelis, D.I., Vonatsos, K.N., 1998. Development and experimental validation of analytical thermal models for the evaluation o the depth of laser-treated zones. Appl. Phys. A 76, 435–439.

Rahman, M., Wang, Z.G., Wong, Y.S., 2006. A review on high-speed machining of titanium alloys. JSME Int. J. Ser. C: Mech. Syst. Mach. Elem. Manuf. 49, 11–20.

Rozzi, J.C., Pfefferkorn, F.E., Shin, Y.C., 2000. Experimental evaluation of the laser assisted machining of silicon nitride ceramics. J. Manuf. Sci. Eng.: Trans. ASME 122 (4), 666–670.

Rosenthal, D., 1946. The theory of moving sources of heat and its application to metal treatments. Trans. Am. Soc. Mech. Eng. 68, 849–866.

Singh, R., Alberts, M.J., Melkote, S.N., 2008. Characterization and prediction of the heat-affected zone in a laser-assisted mechanical micromachining process. Int. J. Mach. Tools Manuf. 48, 994–1004.

Sun, S.J., Durandet, Y., Harris, J.G., Brandt, M., 2007. Laser assisted machining of titanium:laser preheat model and laboratory trials. CAST CRC, Swinburne University of Technology, CAST Report.

Sun, S.J., Harris, J.G., Brandt, M., 2008. Parametric investigation of laser-assisted machining of commercially pure titanium. Adv. Eng. Mater. 10 (6), 565–572.

Yang, N., Sun, S.J., Brandt, M., 2009. Numerical and experimental investigation of the heat-affected zone in a laser-assisted machining of Ti–6Al–4V alloy process. Mater. Sci. Forum. 618/619, 143–146.